Identifying structural patterns in disordered metal clusters

Jonathan P. K. Doye*
University Chemical Laboratory, Lensfield Road, Cambridge CB2 1EW, United Kingdom
(Received 9 June 2003; published 21 November 2003)

Zinc and cadmium clusters interacting with a Gupta potential have previously been identified as prototypical metallic systems that exhibit disordered cluster structures. Here, putative global minima of the potential energy have been located for these clusters for all sizes up to $N \leqslant 125$. Although none of the usual structural forms are lowest in energy and many of the clusters have no overall order, strong structural preferences have been identified. Many of the clusters are based on distorted oblate Marks decahedra, where the distortion involves the bringing together of atoms on either side of a reentrant groove of the Marks decahedron.

DOI: 10.1103/PhysRevB.68.195418 PACS number(s): 61.46.+w, 36.40.Mr

I. INTRODUCTION

There has been much recent theoretical interest in the possibility that small clusters could have lowest-energy structures that are disordered or amorphous. Examples have been found for model clusters interacting with long-ranged pair potentials[1,2] and a wide variety of metal clusters.[3–17] For some of these examples, these disordered clusters appear at sizes between the magic numbers for the usual icosahedral, decahedral, or face-centered-cubic (fcc) forms, that are typically most stable for materials that are close-packed for bulk,[10,13–15] i.e., the disordered structures are more stable than ordered structures with incomplete outer layers. More interesting are the more extreme examples, where disordered structures are lowest in energy even at the magic numbers of the common structural forms.[3,4,7,8,17] These results would suggest that for these clusters the disordered structures are dominant for the relevant size ranges.

By disordered it is usually meant that the structure has no discernible overall order. Of course, there is still local order, as evidenced by structural probes, such as the radial distribution function, but these usually have forms similar to that for bulk liquids and glasses. Additionally, another common features for these clusters is that there are many other disordered structures that lie very close in energy to the global minimum.

Disordered clusters are most likely to occur when the constraints on the nearest-neighbor distances are weak. Then, the energetic cost for the strain present in the individual nearest-neighbor bonds can be low enough to be offset by other advantageous features of the disordered clusters, such as a low surface energy. For the Morse clusters, this occurs when the potential is long ranged and has a wide soft well.[1,2] For metal clusters, the many-body part of the potential is relatively insensitive to disorder in the nearest-neighbor distances.[18] If the contraction at the surface of the cluster (again due to the many-body forces) is strong, the ordered structures can be sufficiently destabilized to make the disordered structures lowest in energy.[18]

For most of the examples where disordered structures have been found to be lower in energy than the most stable icosahedral, decahedral, and fcc clusters, only a few sizes have usually been considered.[3,4,7,8] So, the possibility remains that at some other sizes the local structural preferences present in the disordered clusters could be assembled in a way that gives rise to a particularly stable structure with overall order. If this were the case, global optimization over a complete range of sizes would then reveal these new structural motifs and magic numbers. This has recently been done for model lead clusters, where, although none of the usual forms are ever lowest in energy and many of the clusters have no apparent overall order, particularly stable high-symmetry clusters were found at some sizes.[11]

Indeed there are general grounds for expecting high symmetry structures to be more prevalent among the global minima, because such structures are likely to have more extreme values of the energy (both high and low).[19] This expectation, in my experience at least, seems to be born out empirically. It is rare that the global optimization of clusters does not reveal ordered high symmetry forms at some sizes. For example, even for potentials which have been designed to favor glassy configurations, global optimization has revealed the presence of unusual, but nevertheless ordered, structures.[20,21]

Here, I wish to examine some prototypical metal clusters that so far have only been found to exhibit disordered structures. For potentials of the Gupta form the dependence of the tendency to disorder on some of the parameters of the potential has been elaborated.[4,18] Of the parametrized metals zinc and cadmium clusters emerged as those with the strongest preference for disorder. This tendency was born out in global optimization studies at sizes where particularly stable fcc, decahedral, and icosahedral structures were possible; as expected, the resulting structures appeared disordered.[7]

In this paper, I will attempt to identify structural patterns for these two cluster systems, in particular searching for new magic numbers and novel types of order. This aim is in a similar spirit to Ref. 22, where possible structural patterns for gold clusters modeled by the Gupta potential have been suggested. To achieve this I have performed global optimization for all clusters with up to 125 atoms. A further aim is to then relate back the identified structural patterns to the form of the potential.

II. METHODS

A. Potential

To model the zinc and cadmium clusters I use a Gupta potential[23] fitted by Cleri and Rosato.[24] The potential energy is given by

$$E = E_{\text{pair}} + E_{\text{embed}} \tag{1}$$

$$= \sum_{i<j} \phi(r_{ij}) + \sum_i F(\bar{\rho}_i), \tag{2}$$

where $\phi(r)$ is a short-ranged pair potential, $U(\bar{\rho})$ is a many-body embedding (or glue) function, and $\bar{\rho}_i$ is defined as

$$\bar{\rho}_i = \sum_j \rho(r_{ij}), \tag{3}$$

where $\rho(r)$ is an ''atomic density'' function.

For potentials of the Gupta form

$$\phi(r) = 2Ae^{-p(r/r_0-1)}, \tag{4}$$

$$F(\bar{\rho}) = -\xi\sqrt{\bar{\rho}}, \tag{5}$$

$$\rho(r) = e^{-2q(r/r_0-1)}. \tag{6}$$

These forms arise from the second moment approximation of a tight-binding Hamiltonian. However, these functions are nonunique. Functions that give exactly the same energy can be constructed by the transformation

$$\phi'(r) = \phi(r) + 2g\rho(r), \tag{7}$$

$$F'(\bar{\rho}) = F(\bar{\rho}) - g\bar{\rho}. \tag{8}$$

This transformation redistributes the total energy between E_{pair} and E_{embed}. When

$$g = \left.\frac{dF}{d\bar{\rho}}\right|_{\bar{\rho}=\bar{\rho}_{\text{xtal}}}, \tag{9}$$

$F'(\bar{\rho})$ has a minimum at $\bar{\rho}_{\text{xtal}}$, where $\bar{\rho}_{\text{xtal}}$ is the value of $\bar{\rho}$ in the equilibrium crystal. This choice is called the effective pair format, and has been suggested as the most natural way to partition the energy between the pair and many-body contributions.[25] In this format, when $\bar{\rho}=\bar{\rho}_{\text{xtal}}$ the pair potential controls the energy change for any change of configuration that does not significantly alter $\bar{\rho}$, hence the name. More specifically, by performing a Taylor expansion about this reference density, one can show that to first order, the change in energy is due to the pair potential. Consequently, it is also a much more helpful format for relating the structure to the form of the potential.

The Gupta potential in this effective pair format becomes

$$\phi_{\text{eff}}(r) = 2Ae^{-p(r/r_0-1)} - \frac{\xi}{\sqrt{\bar{\rho}_{\text{xtal}}}}e^{-2q(r/r_0-1)}, \tag{10}$$

$$F_{\text{eff}}(\bar{\rho}) = -\xi\sqrt{\bar{\rho}}\left(1 - \frac{1}{2}\sqrt{\frac{\bar{\rho}}{\bar{\rho}_{\text{xtal}}}}\right). \tag{11}$$

$\phi_{\text{eff}}(r)$ is a sum of two exponentials, so for $p>2q$ it is repulsive at short range and has an attractive well. The minimum in $\phi_{\text{eff}}(r)$ is at

TABLE I. Parameters for the Gupta potentials of Zn and Cd.

	p	q	A/eV	ξ/eV
Zn	9.689	4.602	0.1477	0.8900
Cd	10.612	5.206	0.1420	0.8117

$$r_{\min} = r_0\left[1 + \frac{1}{p-2q}\ln\left(\frac{Ap\sqrt{\bar{\rho}_{\text{xtal}}}}{\xi q}\right)\right] \tag{12}$$

and is of depth

$$\phi_{\text{eff}}(r_{\min}) = -A\left(\frac{\xi q}{Ap\sqrt{\bar{\rho}_{\text{xtal}}}}\right)^{p/p-2q}\left(\frac{p-2q}{q}\right). \tag{13}$$

As $p\to 2q$ from above, the depth of the well in the pair potential goes to zero. $F_{\text{eff}}(\bar{\rho})$ is quadratic in $\sqrt{\bar{\rho}}$ and has a minimum of depth $-\xi\sqrt{\bar{\rho}_{\text{xtal}}}/2$ at $\bar{\rho}=\bar{\rho}_{\text{xtal}}$.

The Gupta parameters for the Zn and Cd potentials are given in Table I, and the functions ϕ_{eff}, ρ, and F_{eff} are shown in Fig. 1. The shallowness of the attractive well in the effective pair potential of cadmium is particularly

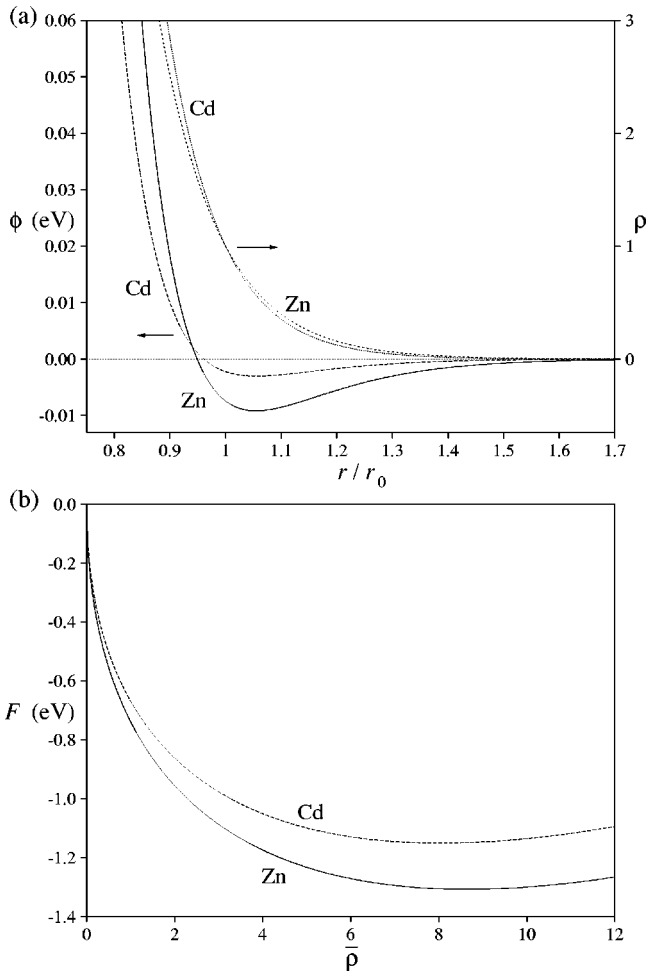

FIG. 1. The three functions that make up the potential: (a) $\phi_{\text{eff}}(r)$, $\rho(r)$, and (b) $F_{\text{eff}}(\bar{\rho})$.

apparent—it is only 0.26% of the depth of the minimum in the embedding function. The pair well depth is somewhat larger for zinc, but it is still only 0.70% of the embedding function minimum. For both systems the shallowness arises because p/q is close to 2.

This feature of the potentials will have similar structural consequences for both systems. First, the majority of the binding energy will come from the many-body interactions. Secondly, the pair potential provides relatively little constraint on the pair distances, except for the repulsion at short distances. Therefore, the most important feature for obtaining a low-energy configuration is to have the individual $\overline{\rho}_i$ values as close as possible to the optimal value. By contrast, there is little energetic advantage in having the nearest-neighbor distances close to the minimum of the pair potential. For a cluster the former can sometimes be more easily achieved through a disordered structure than one based on a lattice, because the additional flexibility of not having well-defined nearest-neighbor distances makes it easier to obtain close to optimal $\overline{\rho}$ values for the surface atoms. This is the source of the tendency to disorder for zinc and cadmium clusters described by the current potentials.

For bulk both zinc and cadmium are hexagonal close-packed with $\overline{\rho}^{\mathrm{Cd}}_{\mathrm{xtal}}=8.042$ and $\overline{\rho}^{\mathrm{Zn}}_{\mathrm{xtal}}=8.638$. These are anomalously low values for close-packed materials. For example, for an ideal close-packed crystal with all nearest-neighbors at r_0, the nearest-neighbor contribution to $\overline{\rho}$ is 12. However, the ratios of the unit cell parameters c/a for the Zn and Cd crystals are particularly large, and so the contribution to $\overline{\rho}$ from nearest-neighbor distances with a component in the c direction is significantly reduced.

The low values of $\overline{\rho}_{\mathrm{xtal}}$ have structural consequences for the clusters. An atom can achieve the optimal $\overline{\rho}$ values with only eight or nine neighbors, so this is possible for surface atoms. By contrast, the nearest-neighbor distances for atoms in the interior need to be elongated to prevent unfavorably large values of $\overline{\rho}$. This is bad news for cluster structures, such as the Mackay icosahedron, where the interior distances are naturally shorter than those on the surface.

The exponential nature of $\rho(r)$ means that significant changes to the $\overline{\rho}$ values can be achieved by relatively small changes to the nearest-neighbor distances. Consequently, it is somewhat easier for atoms, even those with low coordination numbers, to obtain nearly optimal $\overline{\rho}$ values. This behavior contrasts with other many-body potentials, for instance, those produced by the force-matching method,[26] where there is no presumed form for $\rho(r)$, and so more long-ranged functions can result.[26–28]

The current potentials were obtained by keeping the c/a value fixed at the experimental value. This is at some cost in terms of the quality of the fit to other quantities. This led Cleri and Rosato to also construct potentials in which the c/a ratio was allowed to vary in the fitting procedure, and resulted in a better quality fit for many properties.[24] Such a potential is available for cadmium and has dramatically different structural properties because $p/q=3.49$.

B. Global optimization

The global optimization of the zinc and cadmium clusters was performed using the basin-hopping[29,30] (or Monte Carlo minimization[31]) approach. This method has proved particularly successful in locating putative global minima for a wide variety of cluster systems. The nature of the potentials for the current clusters, particularly that $p-2q$ is small, makes global optimization difficult compared to many other metal clusters of similar size. Therefore, a considerable computational effort was required to extend the results up to 125 atoms. It proved particularly important to supplement the standard unbiased runs from random starting points for each size, with short runs started from low-energy minima of nearby sizes with the appropriate number of atoms added or removed. As the structures of the two clusters are similar—seventy of the global minima are the same—it also proved useful to reoptimize the low-energy minima found for one metal for the other. These two types of ''seeded'' runs were applied iteratively until no further new global minima were located.

It should be noted that, of course, there is no guarantee that I have been able to locate the true global minima, and the probability that a global minimum has been missed will increase with cluster size, as the size of the search space, and hence the number of minima,[32–34] increases exponentially with N. Examination of the statistics of how often independent runs locate the same lowest-energy minimum and the importance of the seeded runs can provide one with an idea of the likelihood that the true global minimum has been found. For example, for zinc clusters with less than ninety atoms virtually all the putative global minima were located in unbiased runs, but for $N>100$ the majority of putative global minima were only located in seeded runs. Similarly, for the cadmium clusters virtually all the putative global minima were only located in seeded runs for $N\geqslant 65$. This greater difficulty is because $p-2q$ is closer to zero for cadmium. However, given the similarity of the observed structures for the two metals, I am confident that the vast majority of the putative global minima up to $N=100$ cannot be bettered, but beyond this size one's degree of scepticism about the success of the global optimization should increase rapidly.

III. GLOBAL MINIMA

The energies and point groups for the putative global minima are given in Tables II and III. Point files are available online at the Cambridge Cluster Database.[35] The energies of the global minima are represented in Fig. 2 in such a way that makes particularly stable clusters stand out.

The previous results for these clusters were for a selection of sizes that often show highly symmetric structures, of which energies were reported for $N=13$, 38, 55, 75, and 147.[7] In agreement with that study I also find that none of the common structural forms are lowest in energy at these sizes. More specifically, for $N=13$ and 38 the three lowest-energy minima reported in Ref. 7 are the same as found in the present study. However, for Zn_{55}, Zn_{75}, and Cd_{75} the lowest-energy structures reported by Michaelian *et al.* correspond at

TABLE II. Energies (in eV) and point groups of putative Zn_N global minima.

N	PG	Energy	N	PG	Energy	N	PG	Energy	N	PG	Energy	N	PG	Energy
3	D_{3h}	−3.751296	28	D_{6d}	−37.076416	53	C_1	−70.622509	78	C_1	−104.238674	103	C_1	−137.902829
4	T_d	−5.099346	29	C_2	−38.410947	54	C_1	−71.969642	79	C_{2v}	−105.595357	104	C_1	−139.255744
5	D_{3h}	−6.422287	30	C_1	−39.768212	55	C_1	−73.310032	80	C_{2v}	−106.927940	105	C_1	−140.593303
6	O_h	−7.765873	31	C_1	−41.107234	56	C_1	−74.649595	81	C_s	−108.284296	106	C_1	−141.928489
7	D_{5h}	−9.088519	32	C_1	−42.444864	57	C_1	−75.992628	82	C_s	−109.625208	107	C_1	−143.279843
8	D_{2d}	−10.409083	33	C_1	−43.776617	58	C_1	−77.336947	83	C_s	−110.976689	108	C_1	−144.635048
9	C_{2v}	−11.733002	34	C_3	−45.125218	59	C_1	−78.672227	84	C_s	−112.322650	109	C_1	−145.978993
10	C_{3v}	−13.055156	35	C_s	−46.472931	60	C_1	−80.019432	85	C_1	−113.668080	110	C_1	−147.337545
11	C_2	−14.379679	36	D_{2h}	−47.814946	61	C_2	−81.363067	86	C_{2v}	−115.021815	111	C_2	−148.697585
12	C_2	−15.706971	37	C_1	−49.144718	62	C_1	−82.708058	87	C_{2v}	−116.375101	112	C_1	−150.033337
13	C_s	−17.032142	38	C_s	−50.499983	63	C_1	−84.061400	88	C_{2v}	−117.726908	113	C_1	−151.385243
14	C_{6v}	−18.369312	39	C_{2v}	−51.846864	64	C_2	−85.419385	89	C_s	−119.057698	114	C_1	−152.720206
15	C_s	−19.697479	40	C_s	−53.182148	65	C_1	−86.749702	90	C_s	−120.405576	115	C_2	−154.071651
16	C_s	−21.042019	41	C_s	−54.521834	66	C_1	−88.097872	91	C_{2v}	−121.767147	116	C_1	−155.420956
17	C_{2v}	−22.395676	42	D_4	−55.874358	67	C_1	−89.426800	92	C_{2v}	−123.118340	117	C_1	−156.762711
18	C_{4v}	−23.735972	43	C_4	−57.213737	68	C_1	−90.782264	93	C_s	−124.451825	118	C_1	−158.109816
19	D_{4d}	−25.067563	44	C_s	−58.554345	69	C_1	−92.135925	94	C_s	−125.796431	119	C_1	−159.451202
20	C_{2v}	−26.395373	45	C_{2v}	−59.895318	70	C_1	−93.473840	95	C_s	−127.142167	120	C_{2v}	−160.812498
21	C_s	−27.715028	46	C_s	−61.227348	71	C_s	−94.828826	96	C_{2v}	−128.501419	121	C_1	−162.152965
22	C_{2v}	−29.042499	47	C_s	−62.580198	72	C_s	−96.168254	97	C_s	−129.836679	122	C_1	−163.502185
23	C_1	−30.386460	48	C_s	−63.916581	73	C_s	−97.513085	98	C_{2v}	−131.170669	123	C_{2v}	−164.859277
24	C_2	−31.728122	49	C_{2v}	−65.269233	74	C_s	−98.853247	99	C_s	−132.525475	124	C_1	−166.196591
25	C_2	−33.075590	50	C_s	−66.601903	75	C_{2v}	−100.203580	100	C_{2v}	−133.883827	125	C_1	−167.548063
26	C_2	−34.412179	51	C_1	−67.938575	76	C_1	−101.545341	101	C_s	−135.219057			
27	C_2	−35.744950	52	C_{2v}	−69.281361	77	C_s	−102.900278	102	C_1	−136.566429			

best to the third, eighth, and twenty-second lowest-energy minima, respectively, and lie 0.0031, 0.0186, and 0.0086 eV above the lowest-energy minima reported here. These energies are significant compared to the variations shown in Fig. 2. I did not systematically attempt to optimize 147-atom clusters, as locating the true global minimum for this size would be extremely difficult. However, short basin-hopping runs did find structures that were 0.0966 and 0.0304 eV lower in energy for Zn_{147} and Cd_{147}, respectively, than the lowest-energy structures found by Michaelian *et al.*[7]

Before, we examine the observed structures, there are a number of interesting features evident from Fig. 2. The energy zero in these figures is E_{ave}, a four-parameter fit to the energies of the global minima, where the first two terms correspond to volume and surface energies. For these two clusters the surface term is exceptionally small. The ratio of the surface to the volume coefficient is 7.8% for Zn and 3.3% for Cd. For comparison the value of this ratio is 197% for Lennard-Jones clusters,[36] 48% for Gupta lead clusters,[37,38] 60% for aluminum clusters,[39] and 93, 87, and 63 % for Sutton-Chen silver, nickel, and gold clusters, respectively.[10] One expects the surface energy to be lower for metal clusters than for a cluster interacting with a pair potential, because the lower coordinate surface atoms of a metal can increase their many-body embedding energy by shortening their nearest-neighbor distances. But the Zn and Cd surface energies are very low even for metals, because the optimal value of $\bar{\rho}$ is small enough to be achievable by the surface atoms and the effective pair potential only makes a small contribution to the energy.

The second interesting feature is the magnitude of the fluctuations about the average energy. For Cd and Zn they are again exceptionally small. The average deviation from E_{ave} compared to the average energy per atom is 0.67% for Zn and 0.31% for Cd. For comparison, the value is 16% for Lennard-Jones clusters, 2.1% for Gupta lead clusters,[37,38] and 5.6% for aluminum clusters[39] in the same size range.

The implications of these small fluctuations are that the differences between the more and less stable sizes indicated by Fig. 2 are small, making it more difficult to observe any such ''magic'' numbers. Interestingly, one would expect that the properties of fully disordered clusters would evolve smoothly with size. By this measure, these zinc and cadmium clusters seem to be close to this limit.

We will first examine the zinc clusters in detail, and then later look at the relatively small structural difference between the two systems. A selection of zinc clusters are depicted in Fig. 3 that are either particularly stable or have some interesting structural feature. Up to $N=10$ the structure of the smallest zinc clusters are typical of what one usually finds for clusters modeled by empirical potentials. However, instead of structures leading up to the 13-atom icosahedra, more open structures are then preferred. The example shown in Fig. 3 for Zn_{13} can be considered as a polytetrahedral fragment of a 19-atom double icosahedron. It is insightful to examine why this structure is lower in energy than the 13-

TABLE III. Energies (in eV) and point groups of putative Cd_N global minima. Those labeled with a star have the same structure as the Zn_N global minimum.

N	PG	Energy	N	PG	Energy	N	PG	Energy	N	PG	Energy	N	PG	Energy
3	D_{3h}	−3.391649 *	28	C_2	−32.354453	53	C_1	−61.383718	78	C_1	−90.441924 *	103	C_1	−119.516811 *
4	T_d	−4.556244 *	29	C_1	−33.511796	54	C_1	−62.547483	79	C_{2v}	−91.609644 *	104	C_1	−120.682922 *
5	D_{3h}	−5.710992 *	30	C_2	−34.677431	55	C_s	−63.711040	80	C_s	−92.767096	105	C_1	−121.841138
6	O_h	−6.873544 *	31	C_1	−35.838691 *	56	C_2	−64.871474	81	C_s	−93.931045 *	106	C_1	−123.000416 *
7	D_{5h}	−8.028455 *	32	C_1	−36.999668 *	57	C_1	−66.031560 *	82	C_1	−95.092765	107	C_1	−124.164675 *
8	D_{2d}	−9.182587 *	33	C_1	−38.157466 *	58	C_1	−67.193590	83	C_s	−96.259818 *	108	C_1	−125.323742
9	C_{2v}	−10.337961 *	34	C_1	−39.318659	59	C_1	−68.352805 *	84	C_1	−97.415006	109	C_1	−126.488046
10	D_{4d}	−11.492834	35	C_1	−40.483344	60	C_1	−69.515486	85	C_1	−98.582433 *	110	C_1	−127.654226 *
11	C_2	−12.648250 *	36	D_{2h}	−41.646892 *	61	C_2	−70.678373 *	86	C_1	−99.742283	111	C_2	−128.824065 *
12	C_2	−13.804680 *	37	C_s	−42.803277	62	C_2	−71.838429	87	C_{2v}	−100.912912 *	112	C_1	−129.985671 *
13	C_s	−14.960307 *	38	D_{2d}	−43.967614	63	C_1	−73.002649 *	88	C_{2v}	−102.077956 *	113	C_1	−131.150549 *
14	D_{6d}	−16.116921	39	C_{2v}	−45.132103 *	64	C_2	−74.172601 *	89	C_s	−103.236780 *	114	C_1	−132.311215 *
15	D_3	−17.276238	40	C_s	−46.291870 *	65	C_1	−75.330653	90	C_1	−104.397182	115	C_2	−133.475490 *
16	C_s	−18.434583	41	C_{2v}	−47.451405	66	C_1	−76.493660 *	91	C_{2v}	−105.565322 *	116	C_1	−134.637941 *
17	C_{2v}	−19.600675 *	42	D_4	−48.613389 *	67	C_1	−77.650700	92	C_{2v}	−106.733237 *	117	C_1	−135.800525 *
18	C_{2v}	−20.764865	43	C_4	−49.774701 *	68	C_1	−78.815370 *	93	C_s	−107.892659 *	118	C_1	−136.963187
19	C_{2v}	−21.923540	44	C_s	−50.937992 *	69	C_1	−79.982620 *	94	C_s	−109.048698 *	119	C_1	−138.125231
20	C_{2v}	−23.080283 *	45	C_{2v}	−52.100346 *	70	C_1	−81.143066 *	95	C_s	−110.214298	120	C_1	−139.285228
21	C_1	−24.234793	46	C_s	−53.258607	71	C_1	−82.302019	96	C_s	−111.382493	121	C_2	−140.450672
22	C_1	−25.390380	47	C_s	−54.421794 *	72	C_1	−83.462242	97	C_s	−112.543725 *	122	C_1	−141.614397
23	C_1	−26.552108 *	48	C_s	−55.581917 *	73	C_s	−84.623790 *	98	C_s	−113.703547	123	C_{2v}	−142.780180 *
24	C_1	−27.710728	49	C_{2v}	−56.746239 *	74	C_s	−85.787478 *	99	C_s	−114.863226	124	C_1	−143.938617
25	C_2	−28.875894 *	50	C_s	−57.905181 *	75	C_1	−86.948788	100	C_s	−116.029828	125	C_1	−145.100610 *
26	C_2	−30.036716	51	C_1	−59.063265	76	C_1	−88.112746 *	101	C_s	−117.191782 *			
27	C_1	−31.194825	52	C_1	−60.223182	77	C_s	−89.279311 *	102	C_1	−118.354639 *			

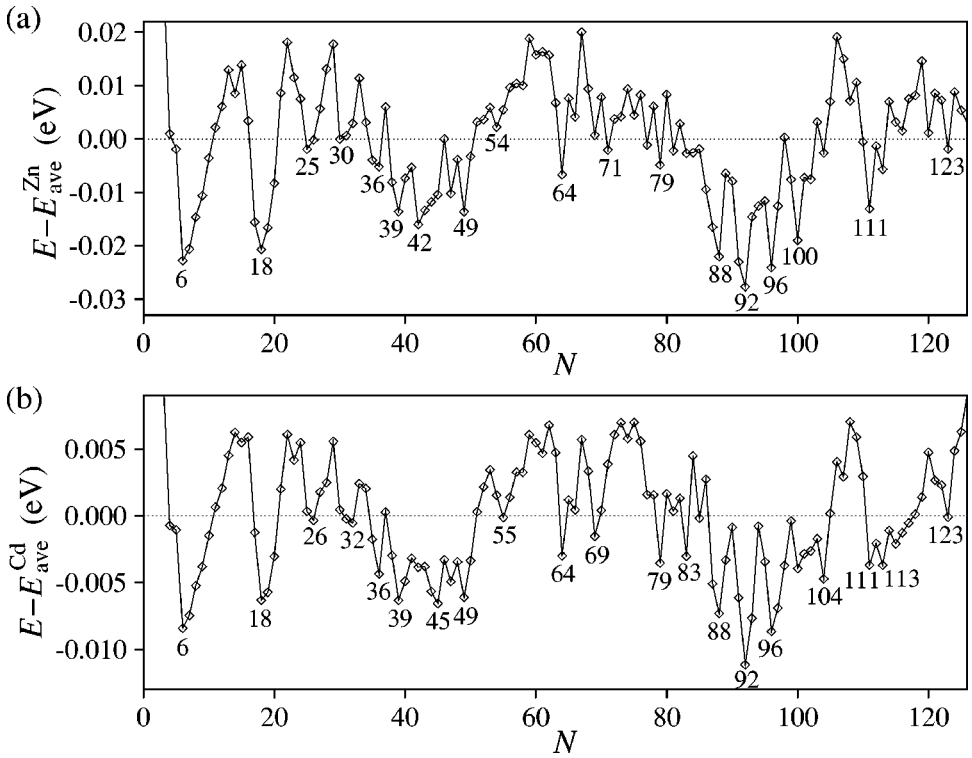

FIG. 2. Energies of the putative global minima of (a) Zn_N and (b) Cd_N relative to E_{ave}, a four-parameter fit to their energies. $E_{ave}^{Zn} = -1.3621\,N + 0.1062\,N^{2/3} - 0.0067\,N^{1/3} + 0.0913$. $E_{ave}^{Cd} = -1.1684N + 0.0391N^{2/3} - 0.0143N^{1/3} 0.0425$.

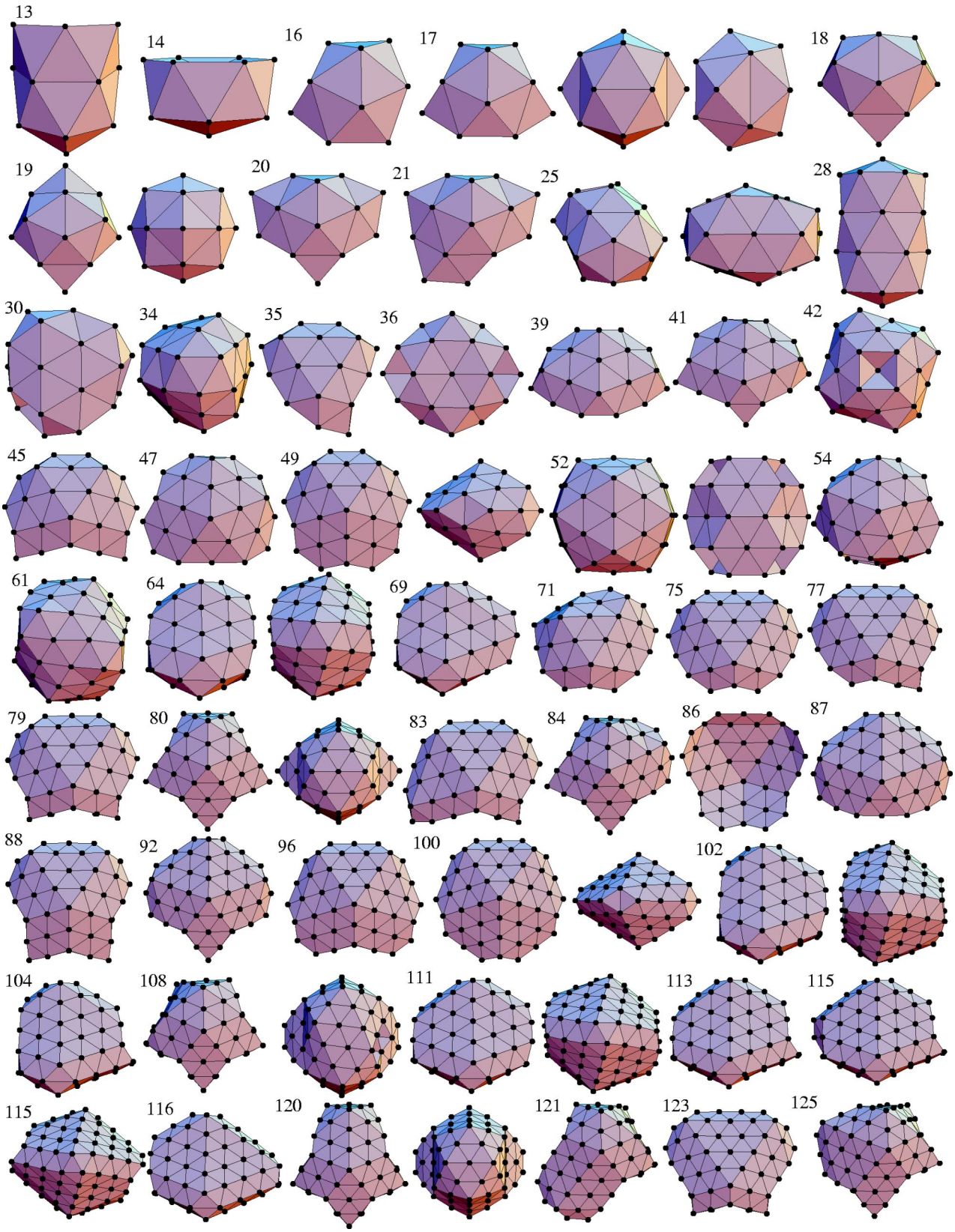

FIG. 3. (Color online) A selection of the putative global minima for Zn_N.

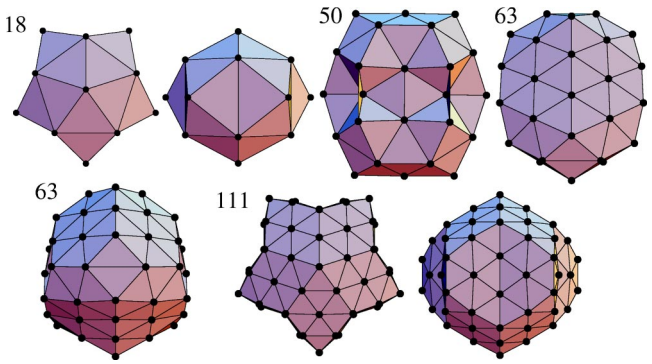

FIG. 4. (Color online) A selection of reference structures for interpreting the Zn_N and Cd_N global minima.

atom icosahedron. The icosahedron is, in fact, 0.335 eV higher in energy, and this stems from an unfavorable embedding energy. The better pair energy, because of the icosahedron's greater average coordination number, does little to offset this. As the distances between the central atom and the vertices of the icosahedron are 5% shorter than the distance between adjacent vertices and $\rho(r)$ increases rapidly with decreasing r, the central atom has an extremely high value of $\overline{\rho}$, namely, 19.568, that is much greater than the optimal value. By contrast, the $\overline{\rho}$ values for all the atoms in the global minimum are relatively close to ρ_{xtal}. This is achieved by the atoms with low coordination number having shorter average distances.

This example illustrates two important features of the potential. First, low-coordinate surface atoms are not disfavored, in contrast to a potential with a strong pair component. Second, it is important that interior atoms do not have short distances. As we will see, it is often much better for an interior atom to have a coordination number larger than twelve since then its nearest-neighbor distances will be longer than those between its neighbors. This latter feature is illustrated by the 14-atom global minimum. The 13-coordinate atom has an average nearest-neighbor separation of $1.052r_0$, whereas the average separation for the nearest-neighbor contacts not involving this atom is $0.958r_0$. Consequently $\overline{\rho}$ for the central atom is only 10.381.

The global minima for $N=16$–21 can all be characterized as distorted decahedral structures. Decahedral structures are based on pentagonal bipyramids (hence the name) and have a single fivefold axis of symmetry. The pentagonal bipyramids themselves are usually not particularly stable because they have a relatively nonspherical shape. By the introduction of reentrant grooves at the five equatorial vertices that are parallel to the fivefold axis, more stable Marks decahedra can be produced.[40,41] An 18-atom example is shown in Fig. 4 that was derived from a 23-atom pentagonal bipyramid, where the introduction of the grooves gives rise to five four-coordinate capping atoms.

This 18-atom Marks decahedron is in fact itself not that unstable and is only 0.042 eV above the global minimum. Even though the central atom is 12-coordinate, this atom is able to maintain a reasonable $\overline{\rho}$ value (9.867), while an expansion of the structure along the axial direction allows the surface distances to contract.

However, the energy can be further improved by distorting this Marks decahedron. The distortion of this decahedra is easy to see for the 17-atom global minimum. This structure can be derived from the Marks decahedron (minus one capping one atom) by a diamond-square-diamond rearrangement,[42] where the contact between the atoms in the groove opposite the missing cap atom is broken and a contact between the adjacent capping atoms is formed (compare the second views of the two structures in Fig. 3 and 4). During this process the two capping atoms are also drawn closer to the central atom to form new contacts, thus giving the central atom a coordination number of 14. The planes containing the two fivefold rings of atoms that were parallel in the Marks decahedron are now splayed apart (see the third view of the Zn_{17} global minimum). It is also noticeable that the structure in the region of the distortion locally resembles the 13-atom icosahedron with the surface atoms now six coordinate.[22] The second view of Zn_{17} looks down a twofold axis of this icosahedral-like region.

The energetic advantage provided through this "groove-bridging" distortion is mainly through the lowering of the energies of the two capping atoms that come into contact. The increase in their coordination number to 6 gives rise to both an increase in $\overline{\rho}$ and a more favorable pair energy. The energy of the central atom is left relatively unaffected, because the increase in coordination number is compensated by an increase in the average nearest-neighbor separation for that atom.

The other global minima for $N=16$–21 can be also understood in terms of this distortion. Zn_{16} simply has one less capping atom than Zn_{17}. For $N=18$ and 19 two of the grooves are bridged, giving rise to a 16-coordinate central atom. The combined effect of the two distortions also causes the contact in the groove adjacent to the these two distortions to be broken, thus giving rise to a square face, which is itself capped in Zn_{19}, and a fourfold axis of symmetry (see the second view of Zn_{19}). Zn_{20} and Zn_{21}, similar to Zn_{17}, are only distorted at one groove; the additional atoms fill in some of the other grooves taking the structure closer towards the 23-atom pentagonal bipyramid.

Such distorted decahedral structures have previously been seen for a number of metal potentials,[10,13,14,22,37,43–45] particularly those that have a tendency to disorder. Indeed, Soler *et al.* have identified such structures as particularly important for amorphous gold clusters, and have used them as a basis to suggest schemes to produce potentially new magic number clusters for larger sizes.[22]

As the size of the clusters increase, so of course must the number of atoms in the interior. Zn_{25} is typical of most of the clusters with two internal atoms. It can be considered as two interlocking distorted decahedra. In the view shown in Fig. 3 a Zn_{18}-like fragment can be clearly seen. The exception to these type of structures occurs at Zn_{28}. The sixfold symmetric structure is a continuation of Zn_{14} and has four stacked hexagonal rings arranged in an antiprismatic fashion. One would expect such a structure to have three internal atoms,

but instead there is a vacancy in the very center of the structure. Again, this is to avoid internal atoms with values of $\overline{\rho}$ that are too large.

Zn_{30} and Zn_{34} are typical of structures with three and four internal atoms. The overall shape reflects the triangular and tetrahedral arrangement of the internal atoms, but it is again hard to detect any overall order. Zn_{36} provides an interesting exception. The surface atoms have basically the same geometry as a recently identified 38-atom polytetrahedral structure.[20,21] However, there are only four (not six) internal atoms, and these are arranged as a planar rhombus.

First at $N=35$ and then from $N=38$ a new series of distorted decahedral structures begins. Again they are based on a Marks decahedron that has been created from a pentagonal bipyramid (in this case with 54 atoms) by introducing reentrant grooves that are one layer deep. A similar mechanism of distortion is again seen. Atoms that are on the equatorial edges of the cluster either side of a groove are drawn closer together, although in this case a contact is not actually formed—the distortion is a diamond-square rather than a diamond-square-diamond process. The clusters at $N=35$, 39, 41, 45, 47, and 49 in Fig. 3 provide examples of structures in this sequence. In most of the examples, two such distortions are present at adjacent grooves, and so the whole edge between these grooves is brought closer to the center of the cluster, forming new contacts with the closest interior atoms. As can be seen for the second view of the complete 49-atom Marks decahedron, this lead to a splaying of the planes of pentagonal rings that would otherwise have been parallel.

For these larger clusters, these distortions represent a smaller perturbation on the overall structure than for $N=16$–21. Indeed, they are barely visible when the cluster is viewed down the quasi-fivefold axis. All that can be seen is a slight opening of the angle at the reentrant groove.

Comparing the energetics of the distorted and undistorted 49-atom Marks decahedron shows that the main improvement arising from the distortion is for the interior atoms. The movement of the equatorial edges involved in the distortion closer to the center of the cluster compresses the rest of the surface somewhat and increases the coordination number of some of the interior atoms. This leads to a structure where the ratio of the nearest-neighbor distances for the interior atoms to those of the surface atoms increases from 1.049 to 1.060. Thus, there is less need for the surface to shrink inwards and compress the core in order to improve the $\overline{\rho}$ values of the surface atoms. Consequently, $\overline{\rho}_{\mathrm{bulk}}$, the average $\overline{\rho}$ value for the interior atoms, decreases from 9.197 to 8.756, i.e., closer to $\overline{\rho}_{\mathrm{xtal}}$, and so the energy of the interior atoms decreases. By contrast the distortion has little overall effect on the energy of the surface atoms. Generally, the atoms in the equatorial plane, especially those close to the distortion, improve their energies, but many of the other surface atoms lose out due to the breaking or stretching of contacts in the axial direction.

This decahedral series of structures is interrupted at $N=42$ and 43 by structures with fourfold symmetry. These clusters are loosely related to the 44-atom fcc octahedron, but with one or two opposite vertices removed. The top half of the cluster is then twisted with respect to the bottom to give a slightly buckled outer layer.

Beyond $N=50$ these groove-bridged Marks decahedra are no longer most stable. Instead, there is a size range where the structures typically have no overall order, but where motifs that resemble fragments of Marks decahedra and Mackay icosahedra are evident. Zn_{54} provides a typical example, whereas Zn_{52} is a structure with more order evident. From one side Zn_{52} has perfect Mackay icosahedral order. What has occurred to the other side can be determined by comparing to the 50-atom incomplete Mackay icosahedron shown in Fig. 4. The two contacts that complete the fivefold rings around the two empty vertices of the Mackay icosahedron have been broken, removing some of the tension in the outer layer of the Mackay icosahedron that makes it so energetically unfavorable.[46] Then two atoms (oriented horizontally with respect to the views in the figures) are inserted into the coordination shell of the central atom, increasing its coordination number. Such a structure has previously been located for Au_{52} modeled by a Sutton-Chen potential.[10]

From the particularly stable structures based on the 18-atom and 49-atom Marks decahedra, it is not surprising that there is another series of particularly stable clusters leading to the 100-atom Marks decahedron (Fig. 2). Again this Marks decahedron is formed from a pentagonal bipyramid by the introduction of grooves of depth one layer. More generally, one can use this trend to predict sizes at which particularly stable clusters could potentially occur outside the size range of this study. The sizes for such complete Marks decahedra are given by

$$N=\frac{5}{6}n^3+5n^2+\frac{61}{6}n+2, \tag{14}$$

where n is the number of atoms on an equatorial edge of the Marks decahedron. This gives $N=18,49,100,176,282,\ldots$.

The first of this set of groove-bridged decahedral structures occurs at $N=75$ and the last at $N=101$. Representative examples at $N=75$, 77, 79, 83, 86–88, 92, 96, and 100 are shown in Fig. 3. At the smallest sizes the decahedra are still quite asymmetric. From Fig. 2 one can see that the particularly stable sizes occur at $N=100-4m$, where $m=0$–3. These structures can be formed from Zn_{100} by the sequential removal of four-atoms from each groove to give structures that have m grooves that are two layers deep. It is interesting to know that the complete Marks decahedron is not in fact the most stable of these structures, but that a slight asymmetry is preferred.

Comparing the energetics of the 100-atom distorted and undistorted Marks decahedra reveals a similar story to Zn_{49}. The main stabilization of the distorted structure is due to the decrease in $\overline{\rho}_{\mathrm{bulk}}$ from 8.875 to 8.789. It is also interesting to analyze the reasons for the stability of structures at $N=88$ and 92 with four-coordinate surface atoms. First, this is because a four-coordinate atom can compensate for its low coordination by having very short nearest-neighbor distances, thus achieving a reasonable ρ value; e.g., 7.519 for Zn_{92}. Secondly, this additional short contact reduces the need for the four surface atoms in contact with the adatom to shrink

inward and compress the adjacent interior atoms. For Zn_{92} the $\bar{\rho}$ values for these atoms only increase by 0.313, despite this extra contact, because the pair separations for the other six contacts have expanded by 2.5%.

The structures at $N=63$—70 are also closely based on the 100-atom Marks decahedron, but with a further distortion. From the first view of Zn_{64} one can see the resemblance to the 63-atom structure in Fig. 4 that is an asymmetric fragment of the 100-atom distorted Marks decahedron. The second view of Zn_{64} shows the two-fold axis. From the equivalent view of the 63-atom structure, it is clear that an extra atom has been added to the column of three capping atoms (at the bottom of the first view and in a vertical line in the center of the top half of the cluster in the second view), and then a small twist has been given to the two halves of the structure. Zn_{69} has basically the same structure but with an increase in the size of one of the decahedral faces.

Based on the favorability of small distorted Marks decahedra (similarly to those we see at $N=16$–21) for gold clusters modeled by a Gupta potential, Soler *et al.* suggested a means for using this structural pattern to generate potentially stable large clusters.[22] A 55-atom Mackay icosahedron can be generated from a 13-atom icosahedron by the addition of atoms at the center of each nearest-neighbor contact. By the same process, an 80-atom structure can be generated from an 18-atom distorted Marks decahedron with one of the grooves bridged. Soler *et al.* envisaged that this structure would be most stable when the three four-coordinate atoms in this 80-atom structure were removed.[22] However, the suggested structure is actually the global minimum for Zn_{80}, reflecting the stabilization of low-coordinate atoms that is possible for this potential.

An alternative way to generate the Zn_{80} structure is to introduce reentrant grooves two layers deep into the 100-atom pentagonal bipyramid. This Marks decahedron is then distorted to produce four new contacts that bridge the two capping square pyramids adjacent to a groove. This distortion is analogous to that for bridging a groove one layer deep. In the region of the distortion, the structure looks locally similar to a 55-atom Mackay icosahedron.

Bridging a groove that is two layers deep is generally less favorable than bridging one that is one layer deep. There are only five examples for $N \leqslant 100$. The others occur for Zn_{71-73} and Zn_{84}. Zn_{71} and Zn_{84} are quite interesting because they involve distortions of grooves that are both one and two layers deep. For example, Zn_{84} can be formed from Zn_{80}, by first filling in one of the grooves, so that it is then only one layer deep and then applying the distortion to this groove.

After the completion of the previous decahedral series associated with the Marks decahedra at $N=18$ and 49, there are size ranges where the majority of clusters have no discernible overall order at $N=22$–34 and $N=51$–62, before structures based on the next Marks decahedron become lowest in energy. However, even though the next complete Marks decahedron is at $N=176$, beyond $N=101$ structures based on this larger Marks decahedron are immediately lowest in energy. From $N=102$–117 (excepting $N=108$) the zinc clusters are asymmetric groove-bridged decahedra with the same twist distortion as that for $N=63$–70. As for Zn_{64} this leads to structures with a twofold axis of symmetry at $N=111$ and 115 (see the second views of these structures in Fig. 4).

The first global minima that are fragments of the 176-atom Marks decahedron with only distortions bridging grooves one layer deep occur at $N=122$ and 123. There are also a number of structures, where grooves two layers deep are bridged; e.g., $N=108$, 120, 121, and 125. The structures at $N=108$, 121, and 125 are slightly more complicated, because the reentrant {111} faces in the grooves of the undistorted Marks decahedra are not triangular but instead have two atoms along the outer apical edge. This is illustrated for Zn_{108}, which is based on the 111-atom Marks decahedron shown in Fig. 4. On bridging this groove, it is favorable to remove three atoms that lie on the σ_h mirror plane of the Marks decahedron, and to twist the top and bottom of the cluster slightly to remove a small {100}-type face that would otherwise result.

As has already been noted, for just over half the cadmium clusters in the size range considered, the global minima have the same structures as the zinc clusters. A selection of examples where the global minimum differs from zinc are depicted in Fig. 5. The global minima are again dominated by distorted Marks decahedra, although the positions of capping atoms (e.g., Cd_{16} and Cd_{19}) or the number of grooves that are bridged (e.g., Cd_{100}) may be different. To take Cd_{100} as an example, this structure is second lowest in energy for zinc, because, although it has a better embedding energy than the global minimum, this is more than offset by a worse pair energy. However, because of the reduced magnitude of the pair interactions for cadmium this structure is now lowest in energy.

Another difference between the two systems is the more pronounced stability of the twisted Marks decahedra for cadmium, as indicated by Fig. 2 and the larger size ranges ($N=63$–72 and 102–121) for which these structures are most stable. A further difference is that decahedral structures where grooves of depth two are bridged are less common—there are only three examples for cadmium clusters in the size range considered here.

The least coincidence between the zinc and cadmium global minima probably occurs in the size windows between the series of distorted Marks decahedra where the structures often have no overall order. This probably reflects the large number of disordered structures that only have small differences in energy. Examples of clusters from these size ranges with $N=26$, 30, 38, 55, and 56 are shown in Fig. 5.

IV. CONCLUSION

I have analyzed the structures of the global minima up to $N=125$ for two metallic potentials that have been previously found to have a particularly strong tendency to exhibit disordered clusters.[7] This study confirms that the clusters exhibit none of usual ordered forms for materials that are close packed in bulk. Instead, the majority of the clusters are based on distorted oblate Marks decahedra, but where the distortions are well defined. There are series of structures associ-

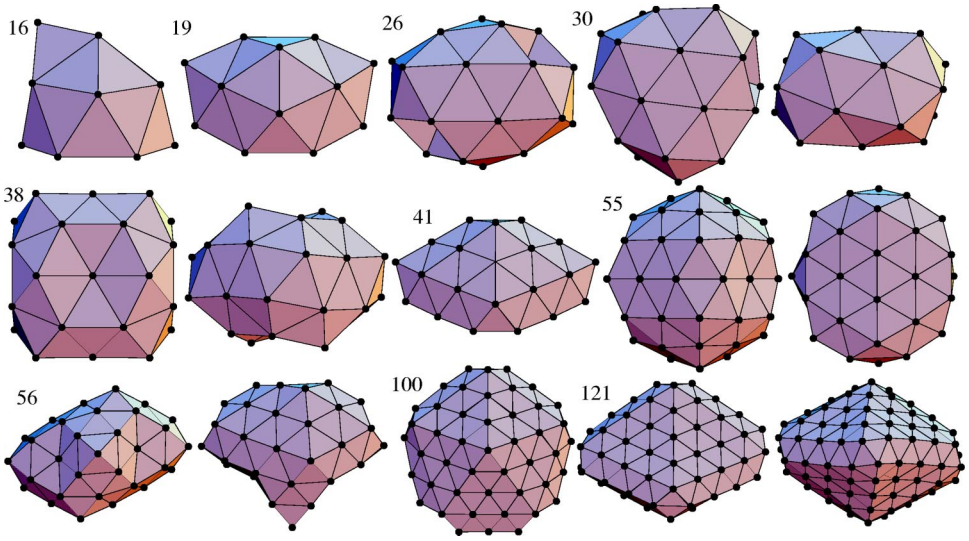

FIG. 5. (Color online) A selection of the putative global minima for Cd_N that differ from those for Zn_N.

ated with the 18-, 49-, 100-, and 176-atom complete Marks decahedra. However, in between there are size windows where the majority of the clusters have no overall order, except for $N>100$ where there is a direct transition between structures based on the 100- and 176-atom Marks decahedra.

Because the effective pair potentials of these zinc and cadmium potentials are very shallow, thus providing relatively little constraint on the pair separations, there is a strong tendency for the surface atoms to contract inwards in order for these atoms to obtain a better many-body embedding energy. The resulting compression of the interior of the cluster causes the conventional structures to be disfavored,[18] because it results in a $\overline{\rho}_{\mathrm{bulk}}$ that is significantly larger than $\overline{\rho}_{\mathrm{xtal}}$. Instead structures for which the nearest-neighbor distances for the surface atoms are naturally longer than those for the interior atoms are likely to be favored, because this allows the difference between $\overline{\rho}_{\mathrm{bulk}}$ and $\overline{\rho}_{\mathrm{surf}}$ to be reduced, bringing them both closer to the optimal value. The distortions of the oblate Marks decahedra help to achieve just this.

This paper should be seen in the context of a growing research program that has sought to understand how the observed structures for metal clusters depend on the form of the many-body potential.[11,18,39,47,48] Interestingly, even for relatively simple potentials of the embedded atom (or glue) form [Eq. (2)] complex structural behavior can result. For example, the current results further highlight how many-body potentials can lead to the stabilization of unusual structural forms.[11,18,22,39,48] Of course, at sufficiently large sizes the bulk structure, in this case hexagonal close-packed, should become most stable, but the energy differences found in this study suggest that the current clusters are far from this limit.

The emphasis in this paper has been on the zinc and cadmium clusters as model systems with a strong tendency to disorder. As noted in Sec. II A, with the Gupta potential it is difficult to capture the large c/a ratio for Zn and Cd without introducing discrepancies for other properties. I have also performed a brief set of global optimization runs using Cleri and Rosato's alternative Gupta potential for Cd, where the c/a ratio was allowed to vary during the fitting. For the selection of sizes I tested the usual ordered forms, i.e., close-packed, icosahedral, and decahedral, were always most stable. Reyes-Nava *et al.* also found these cadmium clusters to have strong first-order-like melting transitions, again reflecting the strong ordering for this alternative potential.[49] Given this strong dependence on the potential parametrization, one should be somewhat sceptical about the abilities of these potentials to provide realistic models for zinc and cadmium clusters. However, the tendency to disorder for these clusters seems to be reproduced by electronic structure calculations using density-functional theory.[7]

There has been little other relevant work with which to compare the current results. Experiments on these clusters have focussed on their electronic shell structure,[50,51] rather than their geometries, and their are only a few theoretical studies to go beyond very small sizes. Electronic structure calculations have been performed for cadmium[52] and zinc[53] clusters with up to 20 atoms. In contrast to the results presented here, these studies found Cd_{13} to be an icosahedron and the larger cadmium clusters to be based upon this structure,[52] and the majority of the zinc clusters to be based upon tricapped trigonal biprisms, albeit often somewhat disordered.[53] These differences are not surprising, because as the potentials used here have been fitted to the properties of the bulk metal, they are expected to work least well at small sizes, where the clusters may exhibit non-metallic properties.[53] The one similarity was that Zn_{17} had a structure with fourfold symmetry, that is related to Zn_{18} and Zn_{19} for the current potential by the removal of one or two capping atoms, respectively. Ramprasad and Hoagland also studied zinc clusters using a many-body potential of the embedded-atom form [Eq. (2)] but where the effective interactions looked very different from the current Gupta potential.[54] Of the series of candidate structures that they reoptimized, they found icosahedral structures to be lowest in energy.

ACKNOWLEDGMENT

The author is grateful to the Royal Society for financial support.

*Electronic address: jpkd1@cam.ac.uk

[1] J.P.K. Doye, D.J. Wales, and R.S. Berry, J. Chem. Phys. **103**, 4234 (1995).
[2] J.P.K. Doye and D.J. Wales, J. Chem. Soc., Faraday Trans. **93**, 4233 (1997).
[3] I.L. Garzón, K. Michaelian, M.R. Beltrán, A. Posada-Amarillas, P. Ordejón, E. Artacho, D. Sánchez-Portal, and J.M. Soler, Phys. Rev. Lett. **81**, 1600 (1998).
[4] K. Michaelian, N. Rendón, and I.L. Garzón, Phys. Rev. B **60**, 2000 (1999).
[5] I.L. Garzón, C. Rovira, K. Michaelian, M.R. Beltrán, P. Ordejón, J. Junquera, D. Sanchez-Portal, E. Artacho, and J.M. Soler, Phys. Rev. Lett. **85**, 5250 (2000).
[6] A. Taneda, T. Shimuzu, and Y. Kawazoe, J. Phys.: Condens. Matter **13**, L305 (2001).
[7] K. Michaelian, M.R. Beltrán, and I.L. Garzón, Phys. Rev. B **65**, 041403(R) (2002).
[8] I.L. Garzón, K. Michaelian, M.R. Beltrán, A. Posada-Amarillas, P. Ordejón, E. Artacho, D. Sánchez-Portal, and J.M. Soler, Eur. Phys. J. D **9**, 211 (1999).
[9] M.D. Glossman, J.A. Alonso, and M.P. Iñiguez, Phys. Rev. B **47**, 4747 (1993).
[10] J.P.K. Doye and D.J. Wales, New J. Chem. **22**, 733 (1998).
[11] J.P.K. Doye and S.C. Hendy, Eur. Phys. J. D **22**, 99 (2003).
[12] J. Oviedo and R.E. Palmer, J. Chem. Phys. **117**, 9548 (2002).
[13] N.T. Wilson and R.L. Johnston, Eur. Phys. J. D **12**, 161 (2000).
[14] S. Darby, T.V. Mortimer-Jones, R.L. Johnston, and C. Roberts, J. Chem. Phys. **116**, 1536 (2002).
[15] C. Massen, T. V. Mortimer-Jones, and R. L. Johnston, J. Chem. Soc. Dalton Trans. **2002**, 4375.
[16] J. Wang, G. Wang, and J. Zhao, Phys. Rev. B **66**, 035418 (2002).
[17] I. Garzon and A. Posada-Amarillas, Phys. Rev. B **54**, 11 796 (1996).
[18] J.M. Soler, M.R. Beltrán, K. Michaelian, I.L. Garzón, P. Ordejón, D. Sánchez-Portal, and E. Artacho, Phys. Rev. B **61**, 5771 (2000).
[19] D.J. Wales, Chem. Phys. Lett. **285**, 330 (1998).
[20] J.P.K. Doye, D.J. Wales, and S.I. Simdyankin, Faraday Discuss. **118**, 159 (2001).
[21] J.P.K. Doye, D.J. Wales, F.H. Zetterling, and M. Dzugutov, J. Chem. Phys. **118**, 2792 (2003).
[22] J.M. Soler, I.L. Garzón, and J.D. Joannopoulos, Solid State Commun. **117**, 621 (2001).
[23] R.P. Gupta, Phys. Rev. B **23**, 6265 (1981).
[24] F. Cleri and V. Rosato, Phys. Rev. B **48**, 22 (1993).
[25] R.A. Johnson and D.J. Oh, J. Mater. Res. **4**, 1195 (1989).
[26] F. Ercolessi and J.B. Adams, Europhys. Lett. **26**, 583 (1994).
[27] H.S. Lim, C.K. Ong, and F. Ercolessi, Surf. Sci. **269/270**, 1109 (1992).
[28] Y. Mishin, D. Farkas, M.J. Mehl, and D.A. Papaconstantopoulos, Phys. Rev. B **59**, 3393 (1999).
[29] D.J. Wales and J.P.K. Doye, J. Phys. Chem. A **101**, 5111 (1997).
[30] D.J. Wales and H.A. Scheraga, Science **285**, 1368 (1999).
[31] Z. Li and H.A. Scheraga, Proc. Natl. Acad. Sci. U.S.A. **84**, 6611 (1987).
[32] C.J. Tsai and K.D. Jordan, J. Phys. Chem. **97**, 11 227 (1993).
[33] F.H. Stillinger, Phys. Rev. E **59**, 48 (1999).
[34] J.P.K. Doye and D.J. Wales, J. Chem. Phys. **116**, 3777 (2002).
[35] D. J. Wales, J. P. K. Doye, A. Dullweber, M. P. Hodges, F. Y. Naumkin, F. Calvo, J. Hernández-Rojas, and T. F. Middleton, The Cambridge Cluster Database, URL http://www-wales.ch.cam.ac.uk/CCD.html
[36] J.P.K. Doye, M.A. Miller, and D.J. Wales, J. Chem. Phys. **111**, 8417 (1999).
[37] S.K. Lai, P.J. Hsu, K.L. Wu, W.K. Liu, and M. Iwamatsu, J. Chem. Phys. **117**, 10 715 (2002).
[38] J.P.K. Doye, New J. Chem., in preparation.
[39] J.P.K. Doye, J. Chem. Phys. **119**, 1136 (2003).
[40] In many cases, although not for the presents clusters, to produce particularly stable Marks decahedra, as well as the introduction of grooves into the pentagonal bipyramids, it is also important to truncate the equatorial edges to reveal {100} facets.
[41] L.D. Marks, Philos. Mag. A **49**, 81 (1984).
[42] W.N. Lipscomb, Science **153**, 373 (1966).
[43] L.D. Lloyd and R.L. Johnston, Chem. Phys. **236**, 107 (1998).
[44] L. D. Lloyd and R. L. Johnston, J. Chem. Soc. Dalton Trans. **2000**, 307.
[45] A. Sebetci and Z.B. Güvenc, Surf. Sci. **525**, 66 (2003).
[46] The 55-atom Mackay icosahedron is in fact 0.828 eV higher in energy than the Zn_{55} global minimum.
[47] F. Baletto, R. Ferrando, A. Fortunelli, F. Montalenti, and C. Mottet, J. Chem. Phys. **116**, 3856 (2002).
[48] S.C. Hendy and J.P.K. Doye, Phys. Rev. B **66**, 235402 (2002).
[49] J.A. Reyes-Nava, I.L. Garzón, and K. Michaelian, Phys. Rev. B **67**, 165401 (2003).
[50] I. Katakuse, T. Ichihara, Y. Fujita, T. Matsuo, T. Sakurai, and H. Matsuda, Int. J. Mass. Spectrom. **69**, 109 (1986).
[51] M. Ruppel and K. Rademann, Chem. Phys. Lett. **197**, 280 (1992).
[52] J. Zhao, Phys. Rev. A **64**, 043204 (2001).
[53] J. Wang, G. Wang, and J. Zhao, Phys. Rev. A **68**, 013201 (2003).
[54] R. Ramprasad and R.G. Hoagland, Modell. Simul. Mater. Sci. Eng. **1**, 189 (1993).